



OPEN

SUBJECT AREAS:

APPLIED PHYSICS

SENSORS AND BIOSENSORS

Received

4 October 2013

Accepted

17 February 2014

Published

5 March 2014

Correspondence and
requests for materials
should be addressed to
G.W.M. (gwmeng@
issp.ac.cn)

Improved sensitivity of polychlorinated-biphenyl-orientated porous-ZnO surface photovoltage sensors from chemisorption-formed ZnO-CuPc composites

Mingtao Li¹, Guowen Meng^{1,2}, Qing Huang³ & Shile Zhang⁴

¹Key Laboratory of Materials Physics, and Anhui Key Laboratory of Nanomaterials and Nanostructures, Institute of Solid State Physics, Chinese Academy of Sciences, Hefei 230031, P. R. China, ²University of Science & Technology of China, Hefei 230026, P. R. China, ³Key Laboratory of Ion Beam Bioengineering, Institute of Technical Biology and Agriculture Engineering, Hefei Institutes of Physical Science, Chinese Academy of Sciences, Hefei 230031, P. R. China, ⁴High Magnetic Field Laboratory, Chinese Academy of Sciences, Hefei 230031, P. R. China.

We report a new mechanism for the enhancement of porous-ZnO surface photovoltage (SPV) response to polychlorinated biphenyls (PCBs, a notorious class of persistent organic pollutants as global environmental hazard) based on copper phthalocyanine (CuPc) chemisorptive bonding on porous-ZnO. A new ZnO-CuPc composite is formed on the porous-ZnO surface due to the interaction between the surface ZnO and CuPc, with its valence band (VB) energy level being higher than that of the pristine porous-ZnO. So that the efficiency of the photogenerated-electron transfer from the composite VB to the adjacent ZnO's surface states is drastically increased due to the reduced energy gap between the transition states. As a result, the sensitivity of the PCB-orientated SPV sensor is much improved by showing amplified variation of the SPV-signals perturbed by PCBs adsorbed on the ZnO-CuPc@porous-ZnO sensitive material.

Persistent organic pollutants (POPs) pose a constant threat to human health as they are hidden in our surrounding environment with high toxicity and will be there for a long period of time¹. Therefore, much attention has been paid to the development of methods for rapid and sensitive detection and monitoring of POPs²⁻⁴. Versatile POPs-orientated sensors have been invented on the basis of varied mechanisms, such as sensing through electronic⁵, electrochemical⁶, optical^{7,8}, and surface photovoltage (SPV)⁹ signals. In particular, the SPV-based sensor is one of the most promising candidates due to its fast photoelectronic response, high surface sensitivity and simple device structure¹⁰⁻¹².

For the SPV-based sensor, the electron redistribution in the surface states under illumination is one avenue to the SPV formation¹³, and the sensing mechanism is based on the variation of the SPV-signals perturbed by the target analyte molecules. As the target molecules usually interact with the surface of sensing material, the surface states play an important role in SPV-based sensors. Some semiconductor materials such as silicon¹⁴ and ZnO¹⁵ can be utilized to fabricate SPV-based sensors due to their existent surface states induced from surface defects. So, the performance of these materials can be improved through extending the surface defects, commonly by doping^{16,17}. Particularly, ZnO possesses intrinsic defects and additional more defects can also be easily obtained by tuning the crystal growth conditions¹⁸, which may circumvent the sophisticated doping. Therefore, ZnO is an ideal candidate material for SPV-based sensors. However, normally the ZnO's SPV-signal is not very strong for lack of sufficient electrons in ZnO surface states¹⁹, resulting in a low sensitivity for detecting target molecules. Some remedies for this such as doping²⁰ and surface modifying²¹ have been investigated. Thereinto, surface modification is comparatively facile and effective to enhance the SPV response²². As ordinary ZnO is an *n*-type semiconductor due to its intrinsic-defect-induced stoichiometry deviation²³, a stable and visible-light-sensitive *p*-type semiconductor may be a suitable modification material to enhance the electron transfer from the *p*-type medication material to the *n*-type semiconductor ZnO under illumination. Since the surface states usually act as



the charge traps²⁴, so some transferring electrons may be captured in the ZnO's surface states. As a result, the electron population in the ZnO's surface states can be increased significantly, leading to enormously enhanced SPV-signal. As such, copper phthalocyanine (CuPc, C₃₂H₁₆N₈Cu), an organic dye with visible light absorption^{25,26}, is chosen in this work. Actually, CuPc has been extensively investigated in organic and organic/inorganic hybrid optoelectronic devices^{27,28}. In particular, the interfacial characteristic of CuPc/ZnO^{29–31} has gained special attention as one of the important organic/inorganic interface. Although the interaction and electronic structure at the interface have been studied^{32–34}, the underlying mechanism for the interaction at the interface remains unclear. Herein, we develop an effective method to improve the sensitivity of ZnO SPV-based sensors by modifying CuPc on our home-made porous-ZnO. We further demonstrate that a new ZnO-CuPc composite is formed on the porous-ZnO surface (the whole system is denoted as ZnO-CuPc@porous-ZnO) via CuPc chemisorptive bonding, thereby generating more efficient photogenerated-electron transfer at the interface between the ZnO-CuPc composite and the neighboring bare surface of the porous-ZnO. By utilizing the ZnO-CuPc@porous-ZnO instead of bare porous-ZnO in the building of the SPV-based sensor, the sensitivity of the sensor is improved by two orders of magnitude to polychlorinated biphenyls (PCBs), one notorious class of POPs as global environmental hazard.

Results

Firstly, we attempted to enhance the SPV of porous-ZnO by surface modification with CuPc. The results show that the SPV of porous-ZnO is greatly enhanced after CuPc modification, and the optimal CuPc ratio is about 1 wt% (Fig. 1a). The CuPc coverage of 0.5%, 1%, and 5% CuPc modified porous-ZnO can be estimated to be 13.56%, 32.48%, and 64.4% by using N:Zn ratio in XPS data, respectively. The ZnO-CuPc composites increase with boosted CuPc coverage, while the surface states decrease with that due to CuPc chemisorption. The ZnO-CuPc composites and the surface states offer the initial and final states of electron transfer to form SPV, respectively. Therefore, a moderate CuPc modification such as 1% offers optimally the stronger SPV signal. In our previous PCB-orientated porous-ZnO SPV-based sensor, the SPV-signal could be reduced in different degrees through the adsorption of PCBs with different concentrations⁹. We therefore speculate that the enhanced SPV-signal would be of great benefit to improve the PCB response performance of the SPV-based sensor. Then, 1 wt% CuPc modified porous-ZnO (denoted as porous-ZnO:1% CuPc) was used to build SPV-based PCB-orientated sensors for response testing. The PCB77 (3,3',4,4'-tetrachlorobiphenyl, one congener of PCBs) response results display that there exist two linear dynamic ranges of 10⁻⁸ ~ 10⁻⁷ M and 10⁻⁷ ~ 10⁻⁶ M, respectively (Fig. 1b). Especially, the lower limit of PCB77 response concentration reaches to 10⁻⁸ M (Fig. 1b), being two orders of magnitude lower than that of the SPV-based sensors built by using pristine porous-ZnO as sensitive materials (10⁻⁶ M, Fig. 1c).

Ten successive measurements of the sensor's SPV response to PCB77 at different concentrations were investigated in order to evaluate the stability of the sensor. The relative standard deviations were 0.55%, 1.21% and 0.24% corresponding to the measurements of PCB77 at concentrations of 1.30×10^{-8} , 2.08×10^{-7} and 1.00×10^{-6} M, respectively (Table S1), showing that the sensor was stable. The long-term stability of the sensor was tested to 2.08×10^{-7} M PCB77 for 35 days (Figure S1). After the first test, the fresh sensor was stored in the laboratory at room temperature and detected intermittently. The SPV response showed no obvious change during the first 5 days, and only 5% of the SPV response was lost after 1 week. After 35 days, the SPV response still remained above 85% of its initial response, indicating the ability of long-term storage and operational stability of the sensor. Besides, the SPV response can be recovered about 90% of its initial response of the fresh sensor via a 60 min heat at 135°C under 150 Pa pressure, showing that the sensor is readily reusable (Figure S2).

To understand the mechanism of increased SPV-signal and improved PCB sensitivity of the PCB-orientated sensor based on ZnO-CuPc@porous-ZnO, the interfacial atomic interactions and bonding state in ZnO-CuPc@porous-ZnO were characterized by using X-ray photoelectron spectroscopy (XPS), Fourier transform infrared spectroscopy (FTIR), Raman spectroscopy and UV-Vis absorption spectroscopy, respectively.

The interaction between CuPc and porous-ZnO surface was explored by XPS, as shown in Fig. 2. After CuPc modification on the surface of porous-ZnO, Zn 2p and O 1s peaks both shift by 1.2 eV towards higher binding energies (Fig. 2a–b), and Zn LMM Auger spectral peak shifts by 1.1 eV towards lower kinetic energies (Fig. 2c). These results indicate that the valence electronic cloud densities of surface Zn and O decrease for some atoms of CuPc bond there. In the mean time, the Cu 2p, C 1s and N 1s XPS spectra of the porous-ZnO:1% CuPc are almost in accordance with that of the pure CuPc sample (Fig. 2d–f), revealing that not Cu, C, N but H atoms bond to the surface Zn and O atoms. It has been reported that some hydrogen-related species such as Zn–H and O–H can be yielded in ZnO lattice by H atom doping^{35,36} or on the surface of ZnO by H atom adsorption³⁷. Regarding the large size of CuPc molecule, the H atoms of CuPc can hardly enter ZnO lattice. As our home-made porous-ZnO is assembled by many nanoparticles⁹, there would be lots of Zn and O dangling bonds (denoted as Zn– and O–, respectively) on its surface. So the H atoms of CuPc can easily bond to the Zn– and O– on the surface of porous ZnO. Due to the absence of O and Zn atoms at Zn– and O–, the valence electron clouds of Zn– and O– are much nearer their nuclei compared with that of Zn and O in the crystal lattice. However, the bonding electron clouds are far away from the nuclei of Zn and O after H bonding due to the electron-withdrawing effect of H (The electronegativity value of H is 2.1). Therefore the H atoms decrease the valence electronic cloud densities of their bound Zn– and O–. However, which H atoms of CuPc are bonded to Zn– and O–, and how are they bonded? These questions can be addressed by FTIR and Raman spectroscopy measurements.

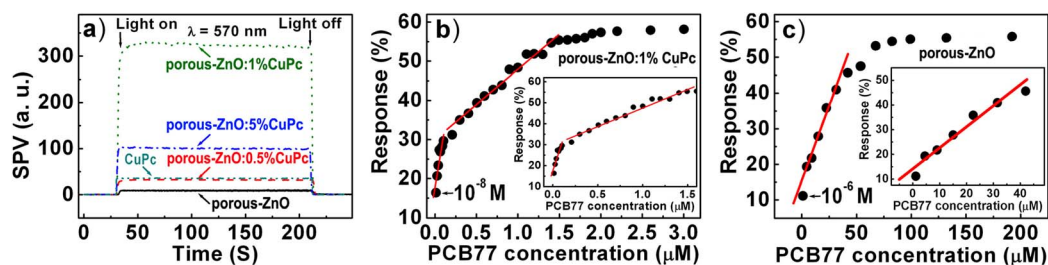


Figure 1 | SPV of porous-ZnO, CuPc, and porous-ZnO modified with CuPc at different ratios (a). PCB77 responses of the SPV-based sensors built from porous-ZnO:1% CuPc (b) and porous-ZnO (c). The straight solid lines are linear fit (b–c). (Insets: PCB77 responses in the linear concentration scales).

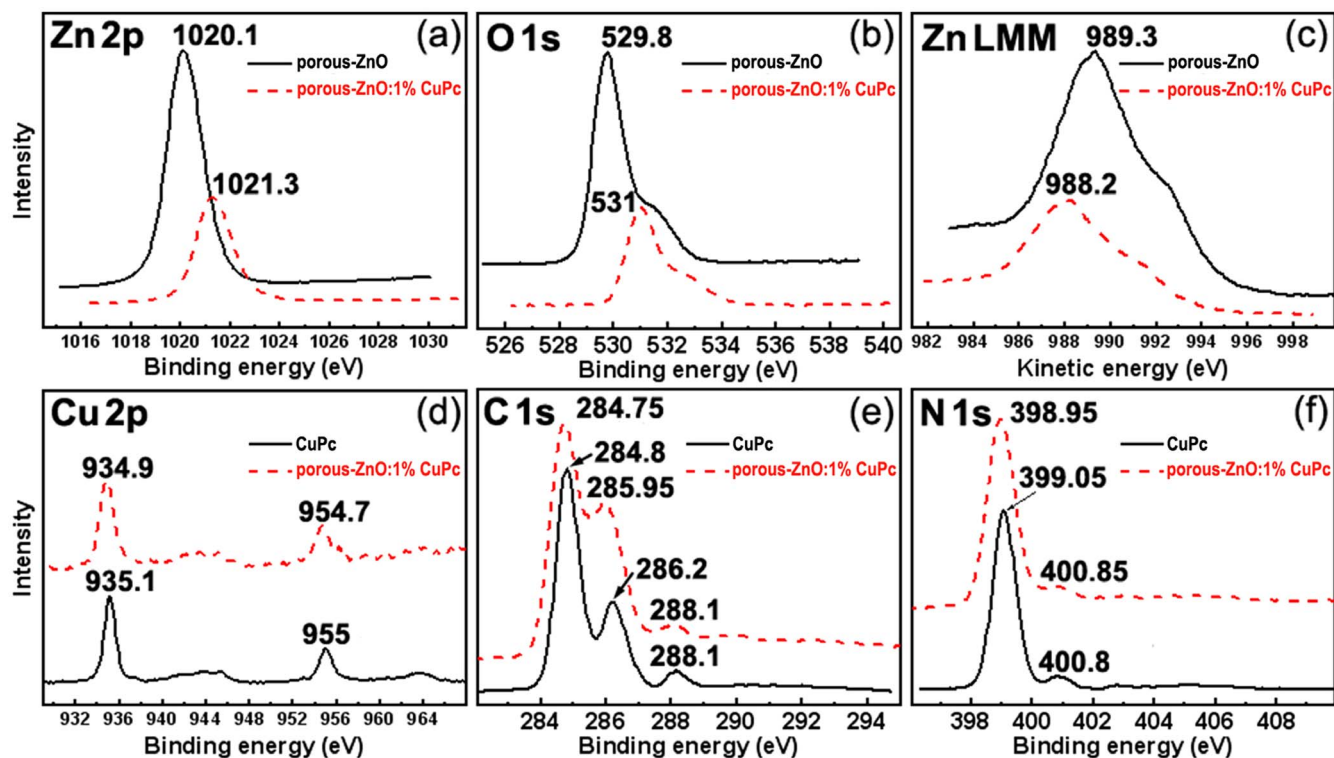


Figure 2 | (a–c) Zn 2p, O 1s XPS spectra and Zn LMM Auger spectrum of porous-ZnO and porous-ZnO:1% CuPc. (d–f) Cu 2p, C 1s and N 1s XPS spectra of CuPc and porous-ZnO:1% CuPc.

Fig. 3a shows the FTIR spectra of porous-ZnO, pure CuPc and porous-ZnO:1% CuPc. To clearly observe the spectral change after CuPc modification on porous-ZnO, the FTIR spectrum of porous-ZnO:1% CuPc was also examined at a low temperature of 5 K. The FTIR spectral peak of porous-ZnO at 1708 cm^{-1} shifts little while the peak at 3125 cm^{-1} shifts by 30 cm^{-1} towards higher wavenumbers after CuPc modification at 300 K and especially shifts by 73 cm^{-1} at 5 K. As the peaks at 1708 cm^{-1} and 3125 cm^{-1} are assigned to Zn–H and O–H vibrations respectively³⁸, therefore the little change of Zn–H vibration (1708 cm^{-1}) indicates that most of Zn–H bonds have been formed in the crystal lattice of porous-ZnO as H atoms doping in O vacancies during the crystal growth, and very few Zn–H bonds are formed on the porous-ZnO surface by bonding the H atoms of chemisorptive CuPc (Fig. 3b, Type I). And the remarkable change of O–H vibration (3125 cm^{-1}) shows that most of O–H bonds are formed on the porous-ZnO surface by bonding the H atoms of chemisorptive CuPc after modification (Fig. 3b, Type II). The Raman spectra

(Fig. 3c) of pure CuPc and porous-ZnO:1% CuPc demonstrate that some peaks (1141.3 , 1335.6 , 1448 , 1520.5 and 1585.7 cm^{-1}) obviously shift (1148.3 , 1344.1 , 1454.8 , 1532.2 and 1597.3 cm^{-1} , respectively) after CuPc modification. These peaks correspond to the vibrations of C_{β} – C_{β} – C_{γ} , C_{β} – C_{β} , C_{α} – C_{β} , C_{δ} – C_{γ} , and C_{δ} – C_{γ} in CuPc molecules, respectively³⁹. According to the experiment and calculation results of CuPc Raman spectra in Ref. 39, we propose that the H@ C_{γ} bound to Zn– or O– can cause the obvious change of all the above-mentioned vibrations (see the H atoms marked with dashed circles in Fig. 3b). Besides, due to the stack pattern of planar CuPc molecules⁴⁰, the H atoms of CuPc can easily contact to the porous-ZnO surface. As the distance between the two neighboring Zn (O) atoms in the Zn–, O– and mixed-terminated ZnO [(0001), (000 $\bar{1}$) and (10 $\bar{1}$ 0), respectively] surface is about 0.4 nm, which matches that of the two neighboring H@ C_{γ} ($\sim 0.5\text{ nm}$). So the two neighboring Zn–(O–) bond the two neighboring H@ C_{γ} of CuPc to form the ZnO–CuPc composite on the porous-ZnO surface.

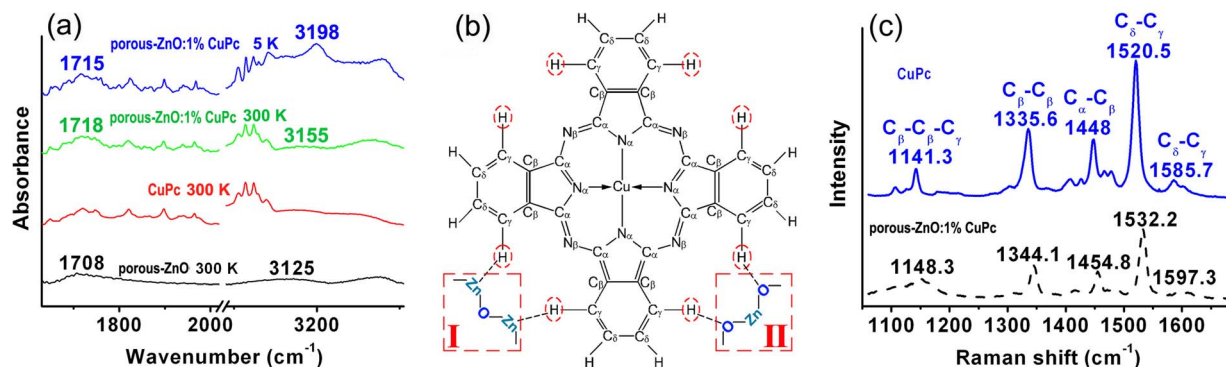


Figure 3 | (a) FTIR spectra of porous-ZnO, CuPc and porous-ZnO:1% CuPc at 300 K, and that of porous-ZnO:1% CuPc at 5 K. (b) Schematic drawing of the CuPc molecular structure and the H bonding patterns. The bound H atoms and their bonding patterns (types I and II) marked with dashed circles and squares, respectively. (c) Raman spectra of CuPc and porous-ZnO:1% CuPc.



Fig. 4a shows the valence band (VB) XPS spectra of the porous-ZnO, pure CuPc and CuPc-modified porous-ZnO, respectively. In fact, XPS spectra mainly reflect the surface properties of these solid powder samples. Therefore, the above measurement results of the CuPc-modified porous-ZnO can be approximately regarded as those of the ZnO-CuPc composite. In XPS measurements, a sufficiently large acceptance angle for detection of emitted photoelectrons is used so that the angle-integrated VB density of states (VB-DOS) can be measured at low photoemission intensity⁴¹. The VB XPS spectrum can be obtained according to the proportional relation between the VB and the VB-DOS. A rather sharp onset of the VB-DOS occurs around the valence band maximum (VBM), however, it can be broadened by instrumental resolution⁴². So the position of the VBM is calculated by extrapolating a linear fit to the leading edge of the VB XPS spectrum to the baseline in order to take account of instrumental resolution induced tail^{43,44}. The VBM of the porous-ZnO and ZnO-CuPc composite, and the highest occupied molecular orbital (HOMO) of the pure CuPc are determined to be 2.19, 3.32 and 2.01 eV, respectively (Fig. 4a inset). We also examined the VB XPS spectra of the porous-ZnO samples modified with CuPc at different ratios, and the results show that the VBM of the ZnO-CuPc composite gradually rises with the increase of CuPc (Fig. 4b), indicating that the VBM of the porous-ZnO rises after CuPc modification. The band gaps of the porous-ZnO, pure CuPc and ZnO-CuPc composite can be estimated to be 3.21, 1.60 and 3.15 eV respectively, according to their absorption experiments (Fig. 4c)⁴⁵. Therefore, the conduction band (CB) minima can be calculated to be 5.40, 3.61, 6.47 eV for the porous-ZnO, pure CuPc and ZnO-CuPc composite, respectively. Additionally, one of energy levels of surface states arising from surface oxygen vacancies (denoted as V_o) can be estimated to be 4.59 eV according to the photoluminescence spectrum peak (~ 520 nm) of the porous-ZnO. It has been reported that the V_o in the *n*-type ZnO lattice is neutral relative to the lattice because the four surrounding Zn dangling bonds contribute two electrons all together⁴⁶. However,

the surface V_o is positively charged with respect to the lattice due to the decreased electrons donated from the three surrounding Zn dangling bonds. Therefore, the surface states arising from surface V_o can capture electrons. So the diagram of energy levels can be depicted, as shown in Fig. 4d. It can be seen that the energy difference between the ZnO-CuPc composite VB (3.32 eV) and the energy level of the porous-ZnO surface state (4.59 eV) is smaller (1.27 eV) than that between the CuPc HOMO (2.01 eV) and the energy level of the porous-ZnO surface state (4.59 eV). Therefore, under working illumination by visible light at 570 nm, it is ZnO-CuPc composite VB electrons instead of CuPc HOMO electrons that can be easily transferred to the surface states arising from the surface V_o in the adjacent porous-ZnO.

Discussion

The electron-transfer was assumed to be first order reaction, so the electron-transfer rate can be defined by the following formula⁴⁷:

$$\frac{dn_t}{dt} = k_n[\rho_s(N_t - n_t) - n_1 n_t]$$

where ρ_s is the density of transferring electrons, N_t is the total surface state density, n_t is the electron-populated surface state density, n_1 is the emission constant and k_n is the capture rate constant.

For the pristine and CuPc-modified porous-ZnO, ρ_s is the density of electrons in ZnO CB and ZnO-CuPc composite VB, respectively. The electron density in ZnO-CuPc composite VB is obviously higher than that in ZnO CB, therefore the electron-transfer rate in CuPc-modified porous-ZnO is higher than that in pristine porous-ZnO, resulting in an obviously increased electron population in the surface states, i.e. a remarkably enhanced SPV-signal (see the left in Fig. 5). In point of the SPV-based PCB-orientated sensor, PCBs can be preferentially adsorbed onto the surface V_o due to the promoted adsorption probability induced by the defects⁴⁸ (see the right in Fig. 5), which reduces the electrons transferred to the surface V_o . As a result,

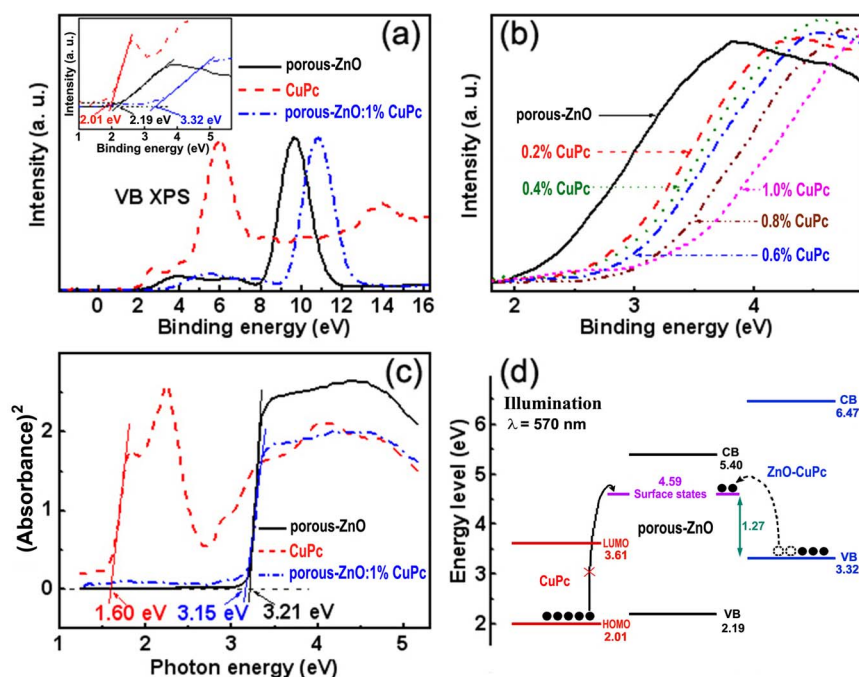


Figure 4 | (a) The VB XPS spectra of porous-ZnO, CuPc and porous-ZnO:1% CuPc. Inset: The straight solid lines show the linear regions, and the VBM can be determined by the intersections of the lines with the baselines. (b) The parts of VB XPS spectra of the porous-ZnO modified with different amount of CuPc. (c) Absorbance squared versus photon energy for porous-ZnO, CuPc and porous-ZnO:1% CuPc, respectively. The straight solid lines show the linear regions, and the band gaps can be determined by the intersections of the lines with the horizontal axis. (d) Schematic showing the process of the photogenerated-electron transfer from the ZnO-CuPc composite to the adjacent porous-ZnO under 570-nm illumination. The black dots represent electrons.

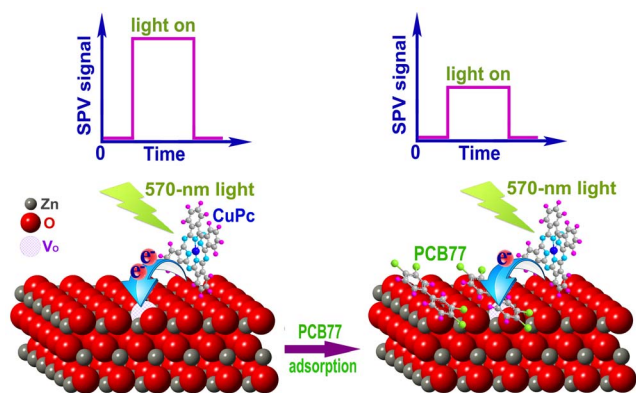


Figure 5 | The schematics for the formation of ZnO-CuPc composite and SPV-signal perturbed by PCB77 adsorption. V_o denotes surface oxygen vacancy.

the SPV-signal drops pronouncedly. The decrement of SPV-related electron transfer disturbed by PCB adsorption is vital to the sensor's sensitivity. For the pristine porous-ZnO built SPV-based sensor, due to the deficient surface-state-electron transition, the decrement of the SPV-related electron transition disturbed by PCB adsorption is very limited, resulting in a higher PCB response concentration limit (10^{-6} M). While for the SPV-based PCB-orientated sensor built by ZnO-CuPc@porous-ZnO, there appears a considerable increment of SPV-related electron transfer, therefore the chance of PCB perturbation is promoted, leading to an enhanced SPV decrement, i.e., a much improved PCB response sensitivity.

In summary, we have investigated the extraordinary SPV property of porous-ZnO modified by CuPc, proved the formation of the ZnO-CuPc composite on the surface of porous-ZnO, acquired enormously enhanced SPV-signals from ZnO-CuPc@porous-ZnO, and as such, achieved a much more sensitive SPV-based PCB-orientated sensor, which has potential in rapid detection of trace PCBs in the environment.

Methods

Synthesis. The porous-ZnO was synthesized by decomposing zinc oxalate precursor⁹. The porous-ZnO microparticles were assembled by many jointed nanoparticles (Figure S3), and the Brunauer-Emmett-Teller (BET) surface area and average porosity determined from the calculated isotherm are 8.11 m²/g and 28%, respectively. The BET pore size distribution ranges from 3.164 to 103.7 nm with a maximum at 36.15 nm and the average pore diameter is 36.53 nm. All the above data were obtained from BET measurement results (Figure S4). To acquire the CuPc-modified porous-ZnO, CuPc powder was firstly dissolved in ethanol, the porous-ZnO was then submerged in the CuPc solution for 6 h. All the dispersal processes were assisted by ultrasonic agitation. The CuPc-modified porous-ZnO powder was obtained by drying at 90 °C under reduced pressure.

Characterization. The absorption spectra were measured with a Shimadzu Solid Spec-3700 DUV UV-vis-NIR spectrophotometer equipped with an integrating sphere. The Raman spectra were recorded on powders with a confocal microprobe Raman spectrometer (Jobin Yvon LABRAM-HR, France). The SPV signals were acquired under visible light illumination with wavelength at 570 nm. All the above-mentioned measurements were performed in air at room temperature. Nitrogen adsorption and desorption isotherm was measured using OMNISORP 100CX Micromeritics. The X-ray photoelectron spectroscopy (XPS) was measured on powders with a thermo ESCALAB 250 spectrometer using an Al K α monochromatized source and a multidetection analyzer under 10^{-8} Pa pressure. The infrared spectroscopy was recorded at a BRUKER VERTEX 80 V Fourier-transform spectrometer with a JANIS-ST100 cryostat under 10^{-6} Pa pressure.

PCB response tests. CuPc-modified porous-ZnO powder was sandwiched between two F/SnO₂ (FTO) conductive glass electrodes connected with a lock-in amplifier to form the sensor platform, as shown schematically in Fig. 6. There was a ~1 mm circular pore in the upside conductive glass for PCB injection. The sensors were tested in a copper shielding box by the light source-monochromator-lock-in detection technique, which referred to the previously reported work^{49,50}. PCB responses of the sensors were measured at the same illumination power density of ~100 mW/cm², and the same temperature of 25 °C and humidity of ~50%.

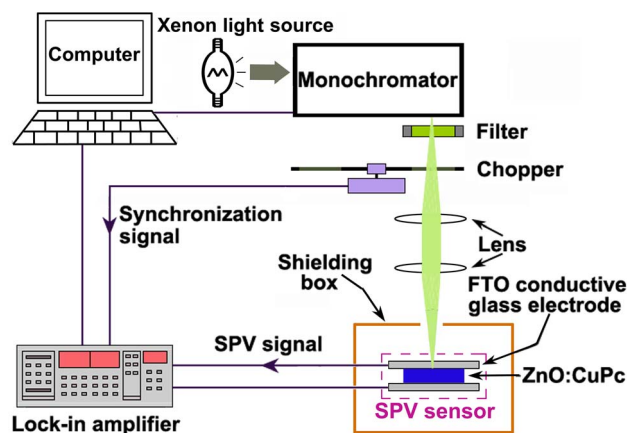


Figure 6 | The schematic diagrams of the SPV sensor and measurement system.

PCB77 solutions (in n-hexane) were injected into the sensors for PCB response tests. To avoid the influence of n-hexane on SPV, the sensors were dried at 80 °C for 30 min after PCBs were injected, and then measured after they were cooled down to room temperature. The positions of the sensors were fixed during the experiments, which makes the comparison of SPV relative value reliable.

The PCB response was defined by the following formula:

$$S = \frac{\Delta V_{bare} - \Delta V_{PCB}}{\Delta V_{bare}} \times 100\%$$

where ΔV_{bare} and ΔV_{PCB} are the time-averaged SPV of the sensor before and after PCB adsorption, respectively.

Two kinds of SPV-based sensors have been fabricated from porous-ZnO:1% CuPc and porous-ZnO, respectively. And their ΔV_{bare} and ΔV_{PCB} with PCB77 adsorption at varied concentrations were measured.

- Jones, K. C. & Voogt, P. Persistent organic pollutants (POPs): state of the science. *Environ. Pollut.* **100**, 209–221 (1999).
- El-Shahawi, M. S., Hamza, A., Bashammakh, A. S. & Al-Saggaf, W. T. An overview on the accumulation, distribution, transformations, toxicity and analytical methods for the monitoring of persistent organic pollutants. *Talanta* **80**, 1587–1597 (2010).
- Salihovic, S. *et al.* A rapid method for screening of the Stockholm Convention POPs in small amounts of human plasma using SPE and HRCG/HRMS. *Chemosphere* **86**, 747–753 (2012).
- Zhu, G., Zhang, X., Gai, P. & Chen, J. Enhanced electrochemical sensing for persistent organic pollutants by nanohybrids of graphene nanosheets that are noncovalently functionalized with cyclodextrin. *Chem. Plus Chem.* **77**, 844–849 (2012).
- Kong, L. *et al.* Novel hybridized SWCNT-PCD: synthesis and host-guest inclusion for electrical sensing recognition of persistent organic pollutants. *J. Mater. Chem.* **21**, 11109–11115 (2011).
- Centi, S., Laschi, S. & Mascini, M. Improvement of analytical performances of a disposable electrochemical immunosensor by using magnetic beads. *Talanta* **73**, 394–399 (2007).
- Mauriz, E. *et al.* Optical immunosensor for fast and sensitive detection of DDT and related compounds in river water samples. *Biosens. Bioelectron.* **22**, 1410–1418 (2007).
- Huang, Z. L. *et al.* Improved SERS Performance from Au Nanopillar Arrays by Abridging the Pillar Tip Spacing by Ag Sputtering. *Adv. Mater.* **22**, 4136–4139 (2010).
- Li, M. T. *et al.* Prototype of a porous ZnO SPV-based sensor for PCB detection at room temperature under visible light illumination. *Langmuir* **26**, 13703–13706 (2010).
- Katsube, T. Highly sensitive immnunosensor with a surface photovoltage technique. *Appl. Biochem. Biotech.* **41**, 59–65 (1993).
- Murakami, Y., Tamiya, E., Uchida, H. & Katsube, T. [Surface Photovoltage-Based Biosensor] [Yang, V. C. & Ngo, T. T. (ed.)] [175–176] (Kluwer Academic/Plenum, New York, 1999).
- Murakami, Y. *et al.* An organic pollution sensor based on surface photovoltage. *Sensor. Actuat. B-Chem.* **53**, 163–172 (1998).
- Kronik, L. & Shapira, Y. Surface photovoltage spectroscopy of semiconductor structures: at the crossroads of physics, chemistry and electrical engineering. *Surf. Interface Anal.* **31**, 954–965 (2001).
- Kanai, Y. *et al.* Integrated taste sensor using surface photovoltage technique. *Sensor. Actuat. B-Chem.* **20**, 175–179 (1994).



15. Zhao, Q. D. *et al.* Photovoltaic properties of a ZnO nanorod array affected by ethanol and liquid-crystalline porphyrin. *Nanotechnology* **19**, 245706 (2008).
16. Yuliarto, B. *et al.* Effect of tin addition on mesoporous silica thin film and its application for surface photovoltage NO₂ gas sensor. *Anal. Chem.* **76**, 6719–6726 (2004).
17. Han, L. N. *et al.* Visible-light-assisted HCHO gas sensing based on Fe-doped flowerlike ZnO at room temperature. *J. Phys. Chem. C* **115**, 22939–22944 (2011).
18. Baruah, S. *et al.* Photoreactivity of ZnO nanoparticles in visible light: Effect of surface states on electron transfer reaction. *J. Appl. Phys.* **105**, 074308 (2009).
19. Zhao, Q. D. *et al.* Surface photovoltage study of photogenerated charges in ZnO nanorods array grown on ITO. *Chem. Phys. Lett.* **434**, 96–100 (2007).
20. Zhai, J. L. *et al.* UV-illumination room-temperature gas sensing activity of carbon-doped ZnO microspheres. *Sensor. Actuat. B-Chem.* **161**, 292–297 (2012).
21. Yang, M. *et al.* Surface photocurrent gas sensor with properties dependent on Ru(dcbpy)₂(NCS)₂-sensitized ZnO nanoparticles. *Sensor. Actuat. B-Chem.* **117**, 80–85 (2006).
22. Kang, D. W. *et al.* Enhanced surface photovoltage response of ZnO nanorod based inorganic/organic hybrid junctions by constructing embedded bulk composite structures. *Appl. Phys. A* **110**, 263–267 (2013).
23. Zhang, S. B., Wei, S. H. & Zunger, A. Intrinsic n-type versus p-type doping asymmetry and the defect physics of ZnO. *Phys. Rev. B* **63**, 075205 (2001).
24. Bubel, S., Mechau, N., Hahn, H. & Schmechel, R. Trap states and space charge limited current in dispersion processed zinc oxide thin films. *J. Appl. Phys.* **108**, 124502 (2010).
25. Bao, Z., Lovinger, A. J. & Dodabalapur, A. Organic field-effect transistors with high mobility based on copper phthalocyanine. *Appl. Phys. Lett.* **69**, 3066–3068 (1996).
26. Lucia, E. A. & Verderame, F. D. Spectra of polycrystalline phthalocyanines in the visible region. *J. Chem. Phys.* **48**, 2674–2681 (1968).
27. Tang, C. W. Two layer organic photovoltaic cell. *Appl. Phys. Lett.* **48**, 183–185 (1986).
28. Takada, J., Awaji, H., Koshioka, M., Nakajima, A. & Nevin, W. A. Organic-inorganic multilayers: A new concept of optoelectronic material. *Appl. Phys. Lett.* **61**, 2184–2186 (1992).
29. Yang, M., Wang, D. J., Peng, L., Xie, T. F. & Zhao, Y. Y. Photoelectric response mechanisms dependent on RuN₃ and CuPc sensitized ZnO nanoparticles to oxygen gas. *Nanotechnology* **17**, 4567–4571 (2006).
30. Karan, S. & Mallik, B. Nanostructured organic-inorganic photodiodes with high rectification ratio. *Nanotechnology* **19**, 495202 (2008).
31. Liu, J. P., Wang, S. S., Bian, Z. Q., Shan, M. N. & Huang, C. H. Organic/inorganic hybrid solar cells with vertically oriented ZnO nanowires. *Appl. Phys. Lett.* **94**, 173107 (2009).
32. Ritz, A., Matz, R. & Lüth, H. Cu-phthalocyanine overlayers on ZnO (1–100) surfaces. *Appl. Phys. A* **33**, 37–41 (1984).
33. Komolov, A. S., Möller, P. J., Mortensen, J., Komolov, S. A. & Lazneva, E. F. Electronic properties of a zinc oxide surface modified by ultra-thin layers of conjugated organic molecules. *Surf. Sci.* **586**, 129–136 (2005).
34. Park, S. H. *et al.* The effect of ZnO surface conditions on the electronic structure of the ZnO/CuPc interface. *Appl. Phys. Lett.* **98**, 082111 (2011).
35. Van de Walle, C. G. Hydrogen as a cause of doping in zinc oxide. *Phys. Rev. Lett.* **85**, 1012–1015 (2000).
36. Lavrov, E. V., Weber, J., Börrnert, F., Van de Walle, C. G. & Helbig, R. Hydrogen-related defects in ZnO studied by infrared absorption spectroscopy. *Phys. Rev. B* **66**, 165205 (2002).
37. Wang, Y. *et al.* Hydrogen induced metallicity on the ZnO(10-10) surface. *Phys. Rev. Lett.* **95**, 266104 (2005).
38. Griffin, G. L. & Yates, J. T. Coadsorption studies of CO and H₂ on ZnO. *J. Chem. Phys.* **77**, 3751–3758 (1982).
39. Basova, T. V. & Kolesov, B. A. Raman spectra of copper phthalocyanin: Experiment and calculation. *J. Struct. Chem.* **41**, 770–777 (2000).
40. Jungyoon, E. *et al.* Effects of substrate temperature on copper(II) phthalocyanine thin films. *Appl. Surf. Sci.* **205**, 274–279 (2003).
41. King, P. D. C. *et al.* Valence-band electronic structure of CdO, ZnO, and MgO from x-ray photoemission spectroscopy and quasi-particle-corrected density-functional theory calculations. *Phys. Rev. B* **79**, 205205 (2009).
42. Piper, L. F. J. *et al.* Valence-band structure of InN from x-ray photoemission spectroscopy. *Phys. Rev. B* **72**, 245319 (2005).
43. Zhang, R. Q. *et al.* Determination of the valence band offset of wurtzite InN/ZnO heterojunction by x-ray photoelectron spectroscopy. *Appl. Phys. Lett.* **91**, 162104 (2007).
44. Chen, X. B., Liu, L., Yu, P. Y. & Mao, S. S. Increasing solar absorption for photocatalysis with black hydrogenated titanium dioxide nanocrystals. *Science* **331**, 746–750 (2011).
45. Matsuoka, T., Okamoto, H., Nakao, M., Harima, H. & Kurimoto, E. Optical bandgap energy of wurtzite InN. *Appl. Phys. Lett.* **81**, 1246–1248 (2002).
46. Janotti, A. & Van de Walle, C. G. Oxygen vacancies in ZnO. *Appl. Phys. Lett.* **87**, 122102 (2005).
47. Morrison, S. R. [Space Charge Effects] [Morrison, S. R. (ed.)] [40–43] (Plenum, New York, 1977).
48. Becker, Th., Boas, Ch., Burghaus, U. & Wöll, Ch. Adsorption probability of CO on a metal oxide: The case of oxygen-terminated ZnO and the influence of defects. *Phys. Rev. B* **61**, 4538–4541 (2000).
49. Lin, Y. H., Wang, D. J., Zhao, Q. D., Yang, M. & Zhang, Q. L. A study of quantum confinement properties of photogenerated charges in ZnO nanoparticles by surface photovoltage spectroscopy. *J. Phys. Chem. B* **108**, 3202–3205 (2004).
50. Wang, D. J. *et al.* Transition identification of tailed porphyrin-Mn(III) complex in the near-UV and near-IR regions using surface photovoltage spectrum. *J. Photochem. Photobiol. A* **93**, 21–25 (1996).

Acknowledgments

This work was supported by the National Key Basic Research Program of China (2013CB934301), Natural Science Foundation of China (11274312, 11175204 and 21107113) and Anhui Provincial Natural Science Foundation (1208085ME86).

Author contributions

M.-T.L. and G.-W.M. designed the experiments. M.-T.L. carried out the major experiments, M.-T.L. and Q.H. analyzed the experimental data. S.-L.Z. performed the FTIR experiments. M.-T.L., G.-W.M. and Q.H. co-wrote the manuscript. All the authors participated in discussions of the research.

Additional information

Supplementary information accompanies this paper at <http://www.nature.com/scientificreports>

Competing financial interests: The authors declare no competing financial interests.

How to cite this article: Li, M.T., Meng, G.W., Huang, Q. & Zhang, S.L. Improved sensitivity of polychlorinated-biphenyl-orientated porous-ZnO surface photovoltage sensors from chemisorption-formed ZnO-CuPc composites. *Sci. Rep.* **4**, 4284; DOI:10.1038/srep04284 (2014).



This work is licensed under a Creative Commons Attribution-NonCommercial-ShareAlike 3.0 Unported license. To view a copy of this license, visit <http://creativecommons.org/licenses/by-nc-sa/3.0>